dynamics

MDPI

Article

Physical Reservoir Computing Enabled by Solitary Waves and Biologically Inspired Nonlinear Transformation of Input Data

Ivan S. Maksymov

Artificial Intelligence and Cyber Futures Institute, Charles Sturt University, Bathurst, NSW 2795, Australia; imaksymov@csu.edu.au

Abstract: Reservoir computing (RC) systems can efficiently forecast chaotic time series using the nonlinear dynamical properties of an artificial neural network of random connections. The versatility of RC systems has motivated further research on both hardware counterparts of traditional RC algorithms and more-efficient RC-like schemes. Inspired by the nonlinear processes in a living biological brain and using solitary waves excited on the surface of a flowing liquid film, in this paper, we experimentally validated a physical RC system that substitutes the effect of randomness that underpins the operation of the traditional RC algorithm for a nonlinear transformation of input data. Carrying out all operations using a microcontroller with minimal computational power, we demonstrate that the so-designed RC system serves as a technically simple hardware counterpart to the 'next-generation' improvement of the traditional RC algorithm.

Keywords: artificial intelligence; chaotic time series; fluid dynamics; nonlinear dynamics; reservoir computing; solitary waves

check for updates

Citation: Maksymov, I.S. Physical Reservoir Computing Enabled by Solitary Waves and Biologically Inspired Nonlinear Transformation of Input Data. *Dynamics* **2024**, *4*, 119–134. https://doi.org/10.3390/dynamics4010007

Academic Editor: Christos Volos

Received: 3 January 2024
Revised: 24 January 2024
Accepted: 3 February 2024
Published: 8 February 2024

1. Introduction

A biological brain is a dynamical system characterised by a complex nonlinear and chaotic behaviour at multiple levels [1–3]. For example, recent theoretical and experimental works have demonstrated that a nerve fibre can operate as a nonlinear waveguide for hybrid electro-acousto-mechanical nerve pulses [4–9]. In particular, it has been shown that an interplay between the nonlinearity of the nerve fibres and dispersion processes occurring in them results in the formation and propagation of solitary waves [5,6].

It is also well known that a biological brain can intrinsically process nonlinear acoustic signals such as natural sounds and music [10–14]. For example, if a human is exposed to a sound with the spectrum that has all of the acoustic frequency components except the fundamental harmonic, their brain restores the missing frequencies automatically. This phenomenon is called restoration of the missing fundamental [15].

In an experiment involving tests of the auditory system of barn owls [16], electrodes were introduced into the animal's brain and the owl listened to a version of Strauss's 'The Blue Danube' made up of tones from which the fundamental frequency had been removed. The researchers hypothesised that, if the missing fundamental harmonic was restored at early levels of auditory processing, neurons in the owl's brain would fire at the rate of the missing fundamental. The experiment confirmed their assumption: the electric output of the electrodes was amplified and played through a loudspeaker, resulting in the original melody of 'The Blue Danube'.

While the biophysical origin of the restoration of the missing fundamental continues to be a subject of debate, it has been suggested that it can be explained by nonlinear and chaotic effects [17]. Nonlinear processes in biological neural systems have also motivated research on artificial neural networks that exploit the nonlinear properties of diverse mathematical models and physical systems [18–29].

Inspired by the natural nonlinear processes in a living biological brain and following the recent advances in the field of reservoir computing (RC)—machine learning algorithms for the prediction of nonlinear and chaotic time series [30–32]—in this paper, we experimentally validated a physical RC system that exploits nonlinear dynamical properties of solitary-like (SL) waves excited on the surface of a flowing liquid film. The resulting neuromorphic computer mimics the functionality of a biological neuron in terms of effectively representing and processing input signals as nonlinear functionals. Yet, it serves as a hardware counterpart to a computationally efficient modification of the traditional RC algorithm called next-generation reservoir computing [33] (in the following, we assume that the traditional RC algorithm is the algorithm proposed in the pioneering works [30,34,35]).

We built and tested a technically simple prototype of the proposed physical RC system employing an inexpensive Arduino microcontroller. While the microcontroller has minimal computational power, but the total cost of the prototype does not exceed USD 100, we argue that, in certain practical situations, the efficiency of the physical RC system may exceed the one of the optimised machine learning software run on a high-performance workstation.

This paper is organised as follows. In Section 2, we survey the traditional and next-generation RC algorithms, as well as overview the recent advances in the field of soliton-based RC systems and adjacent technologies, including analogue and neuromorphic computers based on the nonlinear dynamics of fluids. The technical aspects of the experimental setup used in this work are presented in Section 3. The main results of this paper are presented in Section 4, followed by a general discussion in Section 5.

2. State-of-the-Art

2.1. Traditional Reservoir Computing Algorithm

The traditional RC algorithm stems from two independently developed neural network architectures known as the Echo State Network (ESN) (see Figure 1a) [35] and the Liquid State Machine (LSM) [18]. A neural network architecture similar to the ESN and LSM was also proposed in an earlier work [36] that went mostly unnoticed [37,38].

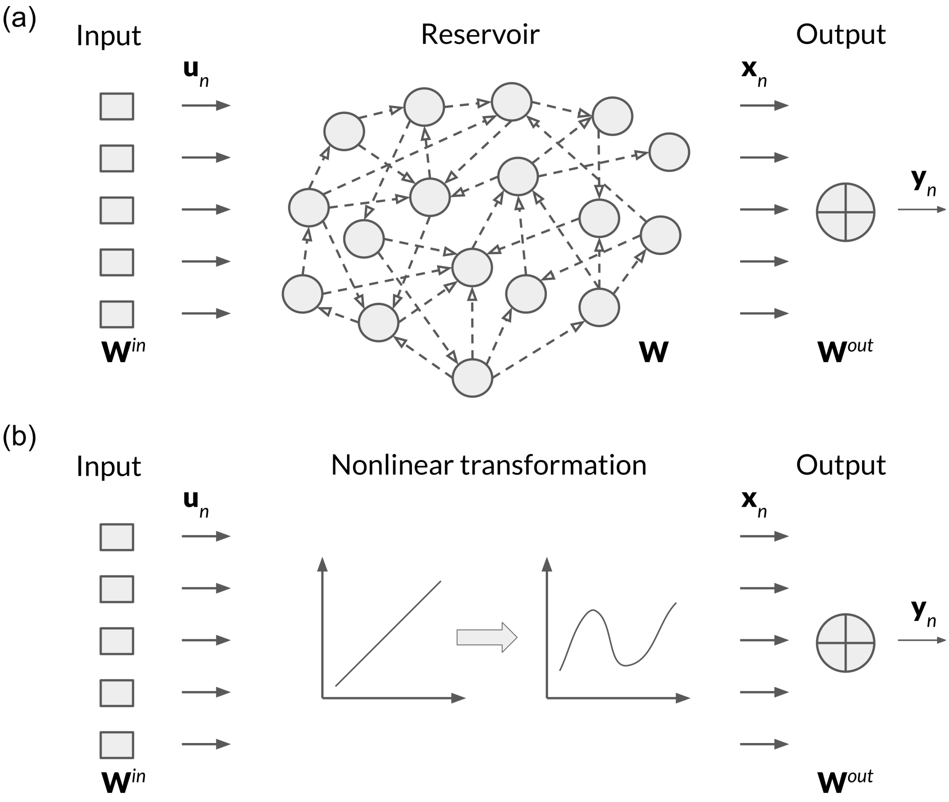

Figure 1. Schematic representation of (**a**) a traditional algorithmic RC system and (**b**) an RC system with a reservoir of random connections substituted by a nonlinear functional of the input data.

A typical RC procedure consists of the following computational steps [30,34,35], where n is the index denoting equally spaced discrete time instances t_n:

1. Create a vector $\mathbf{u}_n$ of N_u input values;
2. Use a random number generator to define an input matrix $\mathbf{W}^{in}$ consisting of $N_x \times N_u$ elements and a recurrent weight matrix $\mathbf{W}$ containing $N_x \times N_x$ elements;
3. Calculate the spectral radius and normalise $\mathbf{W}^{in}$ (see [30,39] for details);
4. Compute a vector $\mathbf{x}_n$ of N_x neural activations as

$$\mathbf{x}_n = (1-\alpha)\mathbf{x}_{n-1} + \alpha \tanh(\mathbf{W}^{in}\mathbf{u}_n + \mathbf{W}\mathbf{x}_{n-1})\,, \tag{1}$$

where the hyperparameter $\alpha \in (0,1]$ controls the update speed of the temporal dynamics (although other activation functions can be used, $\tanh()$ was employed in the seminal works on reservoir computing [30,34,39]);
5. Construct the state matrix $\mathbf{X}$ using the values of $\mathbf{x}_n$;
6. Train the output as $\mathbf{W}^{out} = \mathbf{Y}^{target}\mathbf{X}^{\top}(\mathbf{X}\mathbf{X}^{\top} + \beta\mathbf{I})^{-1}$, where $\mathbf{I}$ is the identity matrix, β is a regularisation coefficient, $\mathbf{X}^{\top}$ is the transpose of $\mathbf{X}$, and $\mathbf{Y}^{target}$ is a matrix composed of target outputs $\mathbf{y}_n^{target}$ for each time instant t_n;
7. Solve Equation (1) with a new set of target data $\mathbf{u}_n$, and compute the output vector as $\mathbf{y}_n = \mathbf{W}^{out}[1;\mathbf{u}_n;\mathbf{x}_n]$.

The computations in Step 7 can be organised differently depending on the particular problem under consideration [39]. In the predictive regime (also known as one-step-ahead prediction), Equation (1) is solved for the target data that were not previously seen by the RC system. However, in the generative regime (also known as the free-running forecast), Equation (1) is solved for an updated target data set given by the output generated by the same RC system at the previous time step (i.e., $\mathbf{x}_n$ is calculated using Equation (1) with $\mathbf{u}_n = \mathbf{y}_{n-1}$). The computer code used in this paper implements the aforementioned traditional RC algorithm, also closely following the ESN code that accompanies Ref. [39].

It is noteworthy that the demonstration of the correct operation in the generative mode is a more-challenging task compared with the operation in the predictive mode and other regimes where the RC system has access to the expected target data. The same applies to various classification tasks and computational tasks that involve target data that correspond to time-delayed training datasets [40]. On the contrary, in the generative regime, the RC system does not know the expected outcome (however, these data can be known to a human operator who is tasked to evaluate the accuracy of the predictions made by the RC system [39,41]). In this context, in the case of the traditional RC algorithm, the operation in generative mode can be compromised by a spurious data point produced by the RC system [39]. While a number of techniques aim to improve the generative mode performance of the algorithmic RC system have been proposed in the literature [39,42], the ability of physical RC systems to operate in generative mode has been difficult to achieve [41,43,44]. In the following, we will demonstrate a possibility to create an efficient physical RC system operating in generative mode.

2.2. Next Generation Algorithmic Reservoir Computing and Adjacent Techniques

To open the discussion in this section, we note that a traditional RC system, defined according to the seminal works [30,34,35], uses a reservoir of random connections. However, alternative reservoir architectures have been proposed, including ring-like reservoir networks [45–47], that do not rely on the effect of randomness in the traditional RC sense. While these and relevant RC concepts [48,49] are important for the field of reservoir computing, their designs deviate from the traditional RC algorithms, and therefore, they are not considered by us as 'traditional' hereafter.

In the paper [33], an alternative RC algorithm was proposed where the state matrix $\mathbf{X}$ of the traditional RC system was substituted by a matrix $\mathbf{X}^{future}$ consisting of future states $\mathbf{x}_n^{future}$ corresponding to the current and time-delayed discrete input data points

$\mathbf{u}_n$ and their nonlinear functionals (for a schematic depiction of such an approach, see Figure 1b). The so-constructed state matrix was then used to calculate $\mathbf{W}^{out}$, thereby avoiding the computationally demanding Steps 2–4 of the calculation procedure outlined in the previous section. Importantly, based on the results presented in Ref. [50], it was also demonstrated that the resulting computational scheme does not only circumvent using the matrices of randomly generated neural connections, but is equivalent to and even more computationally efficient than the traditional RC algorithm. This approach was called next-generation reservoir computing [33,51–54]. Similar algorithms that further improve the performance of RC systems have also been proposed [55].

The nonlinear part of the future states $\mathbf{x}_n^{future}$ can be an arbitrary nonlinear function of the input signal. In Ref. [33], accurate forecasts were made using polynomials. It was also established that it suffices to retain just a few polynomial orders to obtain accurate results. A similar result was obtained in Ref. [56] in the context of quantum reservoir computing, where the authors implemented a nonlinear transformation on the input data, demonstrating that further data processing as per the traditional RC algorithm was redundant.

It is noteworthy that a nonlinear functional of the input data can also be obtained using a physical dynamical system. For example, in Ref. [41], a chaotic times series was used as a signal that drives nonlinear oscillations of gas bubbles trapped in a liquid. Sinusoidal waves are known to be the fundamental excitations that define the dynamics of many nonlinear systems [57]. In the case of a cluster of bubbles in water, the excitation with a purely sinusoidal wave results in the generation of signals that contain the higher-order harmonics of the fundamental frequency. This property was used to create a physical analogue of a traditional RC system that approximates a chaotic time series using a large number of sinusoidal waves with different frequencies and amplitudes.

2.3. *Physical Reservoir Computing Systems Based on Solitary Waves*

Since the traditional RC approach employs the nonlinear dynamics of the mathematical system Equation (1), it was demonstrated that a practicable reservoir could be constructed using a hardware dynamical system [30,31]. Known as the physical RC technique, this approach to computations has been successfully validated, both theoretically and experimentally, resulting in the physical RC systems based on spintronic devices [58,59], quantum-mechanical systems [40,60,61], electronic circuits [31,62], photonic systems [31,43,63], mechanical devices [64], and liquids [38,65–67].

It is also well known that the architectures of some analogue computers used in the 20th Century exploited the nonlinear dynamical properties of liquids [38,68,69] (e.g., the Ishiguro computer was based on the fundamental nonlinear physical processes that govern the dynamics of solitary and tsunami waves). Consequently, both due to prior knowledge and independently, there have been proposals of physical RC systems based on the dynamics of solitary waves [38,44,67,69–74].

Solitary waves propagate with a constant velocity and self-maintain their shape due to an interplay between dispersive processes and nonlinear effects in the medium where they exist [75]. Solitary-like (SL) surface waves that originate from the spatio-temporal evolution of flowing liquid films are a particular class of solitary waves known in the field of fluid dynamics (for a review, see, e.g., [76,77]). Whereas SL waves are similar to other kinds of solitary waves, they possess a number of unique futures [78]. For instance, unlike two Korteweg–de Vries (KdV) solitary waves that can pass through each other without a significant change [79], two SL waves can merge, leading to a more-complex behaviour [78].

The dynamics of both KdV [67] and SL [44] waves have been shown to be valuable for creating a computational reservoir. In the following, we demonstrate that the specific nonlinear properties of SL waves offer an additional degree of freedom to control the dynamics of the reservoir and help reduce the computational effort while generally reproducing the operation of the traditional RC algorithm.

3. Experimental Setup

Figure 2 shows the experimental setup of the proposed RC system, which uses tap water as the operating liquid. The experiment was designed so that the setup enabled both studies of a prototype of the RC system and investigations of the fundamental physical properties of SL waves. In the studies of the RC system, the SL waves were detected using a customised red laser diode–photodetector pair. Independent of the RC system operation, solely to visualise SL waves, an organic fluorescent dye was dissolved in water, and the liquid was illuminated with UV light. A high-speed digital camera was used to record the fluorescence images (Figure 2b). The addition of the fluorescent dye did not change the fluid-mechanical properties of the liquid, nor did it affect the operation of the photodetector. The digital camera was not used in the RC-system-related experiments, and it did not interfere with the operation of the laser diode–photodetector pair.

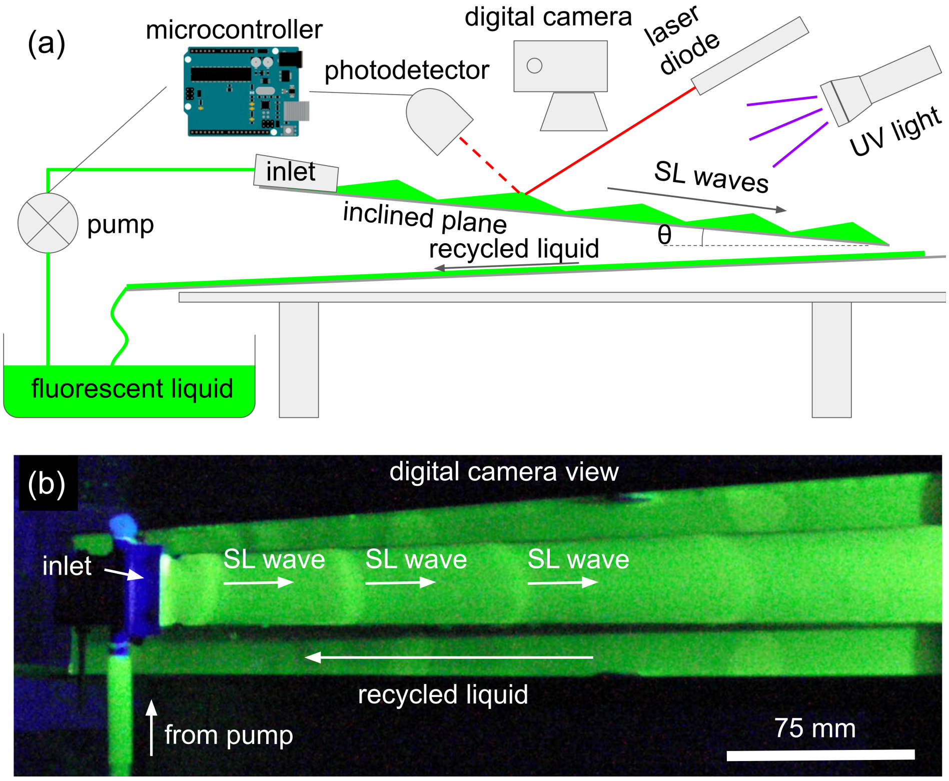

Figure 2. (**a**) Sketch and (**b**) top view fluorescence photograph of the experimental setup used to validate the proposed architecture of the physical RC system. The fluorescent dye, UV light, and digital camera play an auxiliary role and can be removed from the setup without compromising its operation. The remaining components of the setup are controlled by an Arduino microcontroller, which is also used to process the raw data traces. Note that the curvature of the wavefront of SL waves due to the boundary effect does not affect the operation of the RC system since all measurements are taken on the centreline.

The SL waves were excited on the surface of a liquid film flowing along an elongated metal plate inclined with respect to the ground by the angle $\theta = 3^\circ$ [76]. To control the SL waves, the flow rate of the liquid was varied using a miniature electric pump. The electric signal that powered the pump corresponded to the input values $\mathbf{u}_n$ in the algorithmic RC system. To match the temporal dynamics of the input signal with the temporal dynamics of the SL waves, that signal was downsampled so that the fundamental frequency in its spectrum was 1–2 Hz, depending on the particular experimental scenario. The so-controlled pump enabled a smooth variation in the amplitude of the created SL waves.

All components of the setup were controlled by an Arduino UNO R3 microcontroller (16 MHz clock speed, 2 kB RAM, produced by Arduino, Italy) running customised software.

The same microcontroller was used to process the raw experimental data traces and produce the final results. A personal computer was used only to produce the figures presented in this paper.

4. Results

4.1. Formation of the Nonlinear Functional

The nonlinear transformation of the input data implemented in the RC system proposed in this work is illustrated in Figure 1b. To experimentally validate this approach, we chose a simple, but non-trivial test problem [80] of the prediction of the future evolution of a sinusoidal wave. In the framework of our experiment, this scenario corresponds to the excitation of SL waves using the pump, which is driven by a 1 Hz sinusoidal electric signal.

As shown in Figure 3a, each period of the sinusoidal wave triggers the generation of an SL wave (also see Supplementary Video S1). Each SL wave consists of a main pulse with a steep front, which is preceded by a train of secondary pulses of a smaller amplitude [76,78]. When an SL wave moves downstream, the photodetector first receives the light reflected from the secondary pulses, and then, it senses the main pulse. As a result, in Figure 3a, we observe a reversed picture: the train of low-amplitude secondary pulses precedes the main pulse.

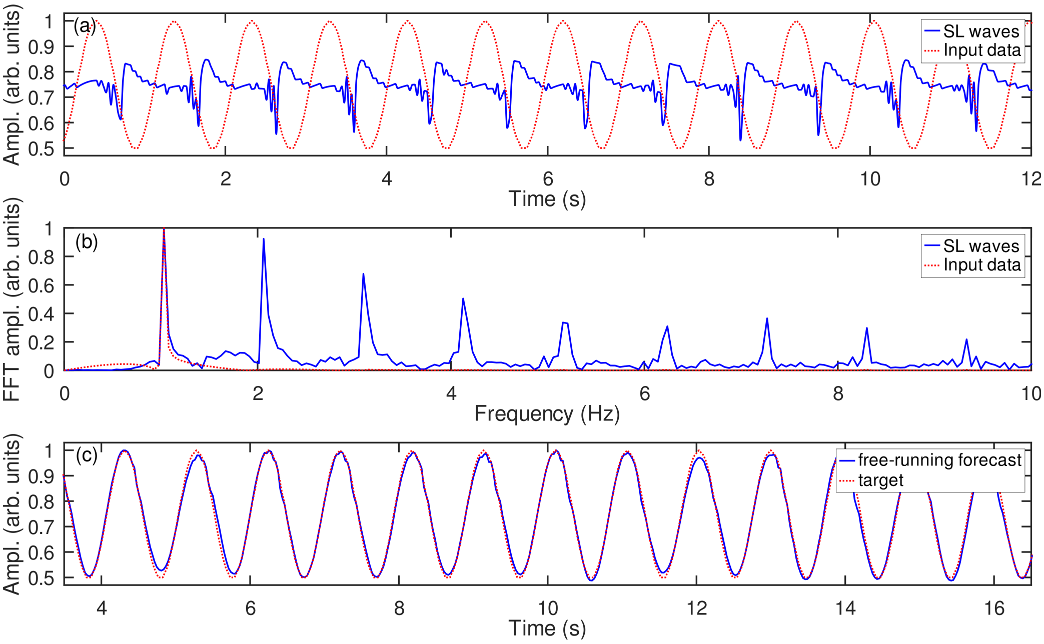

Figure 3. (**a**) Input sinusoidal signal (the dotted curve) and the SL waves excited by it (the solid curve). (**b**) Fourier spectra of the signals in Panel (**a**). (**c**) Free-running forecast of the future evolution of the sinusoidal waves made by the RC system based on the SL waves. Note that the timescale in Panel (**c**) is unrelated to that in Panel (**a**).

We computed the Fourier spectra of both the sinusoidal and SL wave signals and plot them in Figure 3b. We can see that the spectrum of the SL waves is composed of the fundamental (1 Hz) frequency peak and the peaks that correspond to the second, third, fourth, and so on, higher-order harmonics. The spectrum of the sinusoidal wave has only one frequency peak at 1 Hz. Thus, we can see that the SL waves effectively represent the input signal as a nonlinear polynomial function.

Empirically, the nonlinear generation of the higher-order harmonic frequency peaks in Figure 3b can be explained drawing an analogy between the steep front of the main pulse of the SL waves and large-amplitude shock-like acoustic disturbances [76,81]. Shock waves are known to have a frequency spectrum composed of a large number of higher-order harmonic frequencies [82]. A mathematical insight into the nonlinear transformation process can also be gained analysing nonlinear partial differential equations that approximate complex nonlinear physical phenomena [83].

We used the SL wave signal as the vector $\mathbf{x}_n$ of the neural activations of the traditional RC algorithm (Figure 1a). Importantly, although in other physical RC systems, the output of the physical reservoir is also often interpreted as a vector $\mathbf{x}_n$ (see, e.g., [38,59]), in our SL-wave-based RC system, the vector $\mathbf{x}_n$ contains the values that are both time-delayed and a nonlinear function of the input data. Subsequently, this vector is conceptually similar to a future vector used in the next-generation RC algorithm [33]. Moreover, while only the quadratic nonlinear term was retained in Ref. [33] to reduce the computational effort, the use of SL waves enabled us to retain many nonlinear terms, as shown in Figure 3b.

Yet, unlike the original next-generation RC algorithm [33] and its modifications, in our RC system, the vector $\mathbf{x}_n$ is constructed only once as part of the training stage, and it is not updated at the exploitation stage. That is, our algorithm does not follow Step 7 in the traditional RC scheme where Equation (1) needs to be solved. This simplification aligns with the demonstrations of the primary role of the nonlinear transformation of the input data in Refs. [41,56], and it is discussed in more detail in the next subsection.

Figure 3c shows the results of the free-running forecast (generative mode) made by the SL wave physical RC system using the procedure described above. We can see that the RC system correctly predicts the future evolution of the sinusoidal wave. We also note that this result was obtained with minimum post-processing, involving only the removal of the DC component of the output signal.

4.2. Advantages for Generative Mode Operation

Before we test the physical RC system on a more-challenging task of chaotic time series prediction, we discuss one particular advantage of the neuromorphic computation approach introduced in the previous section—making a forecast using neural activations $\mathbf{x}_n$ constructed in the training stage.

In the generative regime, the implementation of Step 7 of the computational procedure outlined in Section 2.1 corresponds to the introduction of a feedback loop from the output of the RC system to its input. Subsequently, the reservoir can be considered to be a self-oscillator [84], which is an established fact [85].

Self-oscillations have been obtained in diverse physical system and mathematical models that involve an oscillator that uses its own output signal to modulate the phase of the external driving force. The so-constructed system can maintain a periodic motion using a source of power that lacks periodicity [84].

We demonstrate that the introduction of a feedback can be avoided without compromising the operation of the RC system. This approach is based on the following facts. A key component of the operation of a trained reservoir is the matrix $\mathbf{W}^{out}$, which remains unchanged at the exploitation stage and is used to make a forecast as $\mathbf{y}_n = \mathbf{W}^{out}[1; \mathbf{u}_n; \mathbf{x}_n]$. From the physical point of view, the chief role of the feedback loop is the maintenance of an appropriate temporal dynamics of the reservoir.

We established that an RC system can produce plausible results when the reservoir is driven by a signal that is similar to the training dataset in terms of temporal dynamics and magnitude. We successfully tested signals corresponding to a delayed version of the training and synthetic signals corresponding to a sum of sinusoidal waves with different frequencies and amplitudes (for a relevant discussion, see [41]). Thus, provided that the dynamics of the reservoir is maintained with an appropriate rate and amplitude, by virtue of the values of $\mathbf{W}^{out}$, the reservoir can produce feasible results.

This finding is especially useful in the case of physical RC systems. Indeed, the introduction of a feedback loop in a computer code that implements the traditional RC algorithm does not present significant technical difficulties [39]. However, in physical RC systems where the dynamics of the reservoir is controlled by an electronic, optical, or opto-electronic circuit [43,63], apart from certain technical limitations, a feedback loop introduces a time delay [43]. Such a delay can be longer than the timescale of the reservoir dynamics, and it can interrupt the dynamics of the reservoir, requiring the application of complex experimental techniques aimed at restoring the intended reservoir dynamics [43]. (We also confirmed that the introduction of an artificial delay in the traditional RC algorithm compromises the operation of the reservoir).

Hence, the technical simplification proposed in this paper enables the developers of physical RC systems to avoid the use of feedback loops, also simplifying the design of the device and decreasing its cost. While any simplification comes at a cost, in the following, we demonstrate that our physical RC system can undertake complex tasks, producing practicable forecasts.

4.3. Free-Running Forecast of Chaotic Time Series

As a next step, we demonstrate the ability of the physical RC system based on SL waves to predict a Mackey–Glass time series (MGTS), which is a standard test problem used to verify the accuracy of neural network models [39,86,87]. While other chaotic time series [33,88–91] have been employed to test both algorithmic and physical RC system, in our previous work [41], we demonstrated that, due to the complexity of the Mackey–Glass model, it suffices to test an RC system using the MGTS to reasonably expect that the same RC system will be able to process other time series with acceptable accuracy.

We generated an MGTS dataset solving the delay differential equation [92]:

$$\dot{x}_{MG}(t) \quad = \quad \beta_{MG}\frac{x_{MG}(t-\tau_{MG})}{1+x^{q}_{MG}(t-\tau_{MG})} - \gamma_{MG}x_{MG}(t)\,, \tag{2}$$

where the overdot denotes differentiation with respect to time and $\tau_{MG} = 17$, $q = 10$, $\beta_{MG} = 0.2$, and $\gamma_{MG} = 0.1$ [39]. Then, we split the resulting dataset into two parts. The first part that corresponds to a few (typically 5–6) pseudo-periods of variation of the MGTS was used to train the RC system. The longer second part was used as the target data that were not known to the RC system, but used exclusively to evaluate the accuracy of the forecast made by the RC system in the generative regime. We underscore that this approach differs from the standard one, where the training and target datasets have the same length, showing that shorter training datasets can be used to train the RC system based on SL waves.

Unlike the SL waves produced by each period of the sinusoidal signal in Figure 3a, the SL waves produced by each oscillation in the MGTS signal have different shapes and amplitudes (Figure 4; for a theoretical analysis, see Ref. [44]). As demonstrated in Refs. [76,77], the SL waves of different amplitude have different propagation speeds. Previously we demonstrated that this physical property enables the SL waves to interact with one with another, resulting in a complex nonlinear dynamical behaviour that is suitable for creating a computational reservoir with a short-term memory [44].

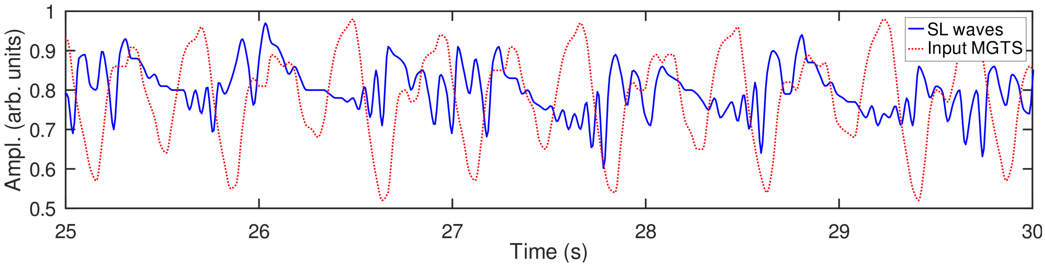

Figure 4. Input MGTS signal (the dotted curve) and the SL waves excited by it (the solid curve). Unlike in Figure 3a, since each variation of the MGTS results in the generation of SL waves with different amplitudes and propagation speeds, the SL waves collide and form more complex wave profiles.

The free-running forecast made by the physical RC system is presented in Figure 5a. In Figure 5b, we also plot the free-running forecast made by the traditional algorithmic RC system implemented following the algorithm presented in Ref. [39]. Both systems were trained and tested on the same training and test datasets, respectively. The hyperparameters $\alpha = 0.3$ and $\beta = 10^{-8}$ optimised for the forecast of the MGTS were used in the traditional RC system (see the code that accompanies Ref. [39]). The spectral radius $\rho(\mathbf{W})$—the maximum absolute eigenvalue of the matrix **W** that scales this matrix to satisfy the echo state property [30]—was increased beyond the standard criterion $\rho(\mathbf{W}) < 1$ to ensure that the reservoir has a longer memory of the input (for an extended discussion of this empirical choice, see Ref. [39]).

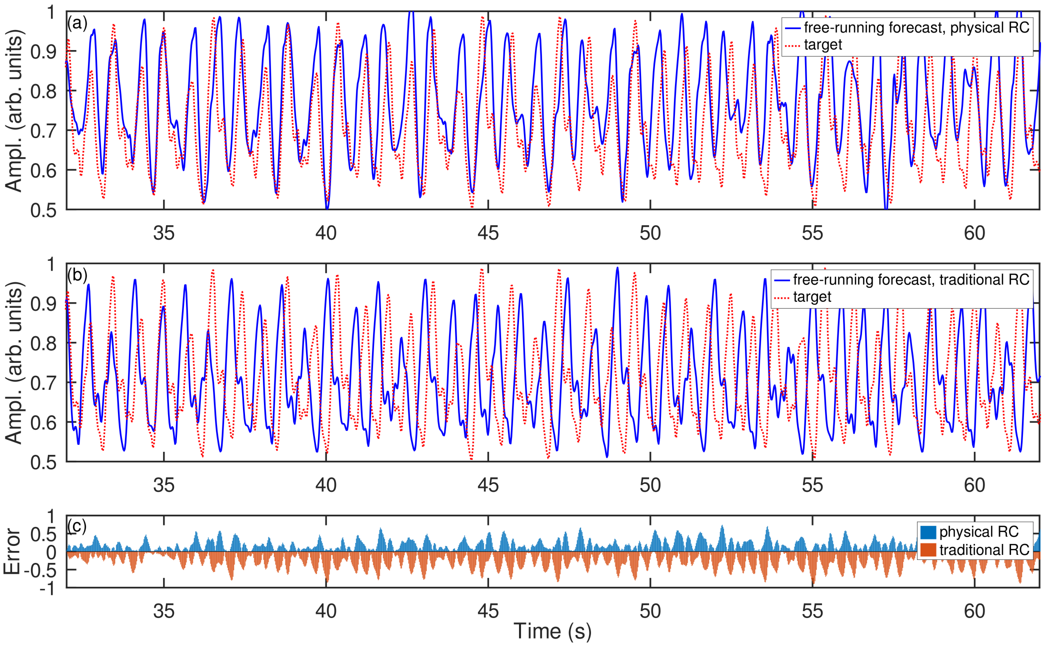

Figure 5. Generative mode operation (free-running forecast) of (**a**) physical RC system based on SL waves and (**b**) traditional algorithmic RC system (the solid curve) compared with the target MGTS (the dotted curve). (**c**) Modulus of the absolute error of the forecasts produced by the physical and traditional RC algorithmic systems. Note that, for the sake of comparison, the error of the traditional RC system is plotted with the negative sign.

It is noteworthy that the traditional RC system requires a much longer training dataset compared with the one needed for the physical RC system. For example, in the ESN software that accompanies Ref. [39] and that is optimised to forecast the MGTS, 2000 data points were used to train the RC system. However, in this paper, we allowed both physical and traditional RC systems to be trained using just 300 data points. In fact, the physical RC system could be trained using an even shorter dataset (e.g., just 100 data points). However, in the particular example shown in Figure 5a,b, the length of the training dataset was increased to 300 data points solely to enable the traditional RC system to make a meaningful forecast (i.e., the algorithmic RC system cannot operate if the training data set is shorter than 300 data points). In these experimental conditions, we also established that, firstly, the traditional RC system requires a reservoir with at least 1000 neurons to produce an interpretable result and, secondly, any further increase in the number of neurons leads to overtraining of the reservoir (the so-called overfitting condition [30]), rendering the RC system unable to reproduce the dynamics of the target time series.

Thus, we can see that the forecast made by the physical RC system reasonably captures the long-term variation of the MGTS in general. Yet, overall, the accuracy of the forecast made by the physical RC is higher than that of the traditional RC algorithm (Figure 5c). We emphasise that, in this test, the traditional RC system used 1000 neurons, and its operation required approximately 2 s of CPU time of a high-performance workstation computer (Apple Mac Studio M1, Ultra 20-core CPU, 128 GB RAM). Of course, taking advantage of the large computational power of a high-performance workstation, using the traditional RC system, we could achieve a more-accurate forecast of the MGTS by increasing the number of both training data points and neurons. However, such a computation was not conducted in this paper since it would violate the equal competition rule between the physical RC system and the algorithmic one.

This analysis made above reflects the well-known fact that, after a certain threshold, any further increase in the size of a computational reservoir results in a small, if any, increase in the performance [32]. The physical RC system presented in this work does suffer from this drawback since it does not rely on random matrices used in the traditional RC algorithm.

The problem of the saturation of the reservoir size also does not exist in the framework of the next-generation RC algorithm [33]. However, software that implements it also requires a modern computer. Yet, the computational effort associated with the next-generation RC computations increases as the nonlinear functional of the input data becomes a higher-order polynomial compared with the quadratic functional used in Ref. [33]. On the contrary, the physical RC system based on SL waves automatically represents the input data using many higher-order nonlinear harmonics and, therefore, does not require any further adjustment of the input datasets.

5. Discussion

5.1. Energy Efficiency, Power Consumption, and Cost

Thus, while a high-accuracy long-term forecast of the MGTS using a traditional RC algorithm requires a high-performance workstation, the result in Figure 5b was obtained using the rather modest auxiliary computational power of an Arduino microcontroller (the Arduino microcontrollers used in the previous demonstration of physical RC systems [93] were not employed to post-process data). Indeed, employing floating point operations per second (FLOPS) as a unit of measure, we estimated the maximum performance of the Arduino microcontroller used in this work to be of the order of 0.1 MFLOPS. For comparison, the workstation computer used to test the traditional RC system can readily deliver more than 2 TFLOPS. Furthermore, the Arduino microcontroller has just 2 kB RAM compared with the 128 GB RAM of the workstation, and the entire experimental setup shown in Figure 2 consumes less than 1 W of power compared with the more than 200 W power consumption by the workstation.

While, in principle, less-powerful workstation models can be used instead of the workstation used in this paper, the cost of a computer with the minimal specification needed to run the software that implements the traditional RC algorithm is around USD 1000, but the power consumed by it is about 50 W. On the contrary, the cost of the prototype of the physical RC system is just USD 100.

To put the cost and power consumption of the physical RC system further into perspective, we note that the price of a mass-produced Akida$^{\text{TM}}$ PCIe Board with a BrainChip neuromorphic processor is USD 499, but an assembled ‘Development Kit’ system based on a personal computer costs USD 9995 and consumes 180 W [94]. Generally speaking, in light of an exponential increase in the computing power demand seen in the last decade [95], the liquid-based unconventional computing system appears to be a plausible alternative to conventional microelectronics [96,97]. Unconventional liquid-state computational systems can also outperform emergent photonics-based computers [98] in terms of energy efficiency since the latter may require high-intensity laser light to induce the nonlinear effects needed for a physical implementation of a neural network [70], but nonlinear processes in liquids can be obtained virtually effortlessly [82].

5.2. Potential Applications

Admittedly, the accuracy of the free-running forecast made by the physical RC system may not be suitable for quantitative analysis such as mathematical modelling of financial markets. Nevertheless, a number of works demonstrated a high value of qualitative forecasts of the variation of financial markets [99,100], which is a finding that aligns with the scope of financial physics, an academic discipline that studies financial markets as physical systems, thus complementing quantitative finance by elucidating the physical nature of financial nonlinear dynamical processes [101].

However, the main advantage of the proposed physical RC system does not necessarily come from its comparison with the computational algorithms used in quantitative research. In fact, the concept of reservoir computing has been applied to study neural information processing in biological brain networks [18,102–105], where the requirement for an RC system to make quantitatively exact forecasts can be relaxed. On the other hand, it is mandatory that the RC system operates similarly to a biological brain. Importantly, this requirement does not only mean a functional resemblance to a brain, but also implies a brain-like energy efficiency [105]. Yet, since it has been suggested that a healthy biological brain relies on the non-randomness of neural connections (i.e., randomness may be associated with some disorders of the nervous system) [106], an RC system that does not use random matrices should serve as a better model of biological neural networks than a traditional RC algorithm.

In this context, the physical RC system based on SL waves has certain advantages. Indeed, firstly, the physical RC system does not rely on randomness, defined in terms of the traditional RC algorithm. Secondly, as discussed in the Introduction, the nonlinearity of SL waves employed in the RC system is physically similar to the nonlinear processes in the nervous system. Thirdly, the physical system is both computationally and energy efficient. Fourthly, it is conceivable that SL waves or other types of solitary waves [6] could be used to create an artificial neuron. The research work in this direction is going on both from the biophysical and chemical [96] and machine learning [102–104] points of view.

It is also noteworthy that biological environments represent significant technological challenges for the developers of implantable brain–computer interfaces and other AI-based systems intended to co-operate with the nervous system of a living organism [107]. These challenges include the impact of various physical processes such as vibrations, scattering, and absorption. Previously, we established that SL waves are highly immune to external mechanical vibrations at the frequencies from 20 to 100 Hz [76]. Therefore, the RC system based on SL waves can also operate in noisy environments. Yet, its ability to make forecasts should not be affected by strong magnetic and electromagnetic fields, which is, for example, a technological challenge for spin–wave-based neuromorphic computers [59,108,109].

Finally, the fields of creative music composition and manipulation of sound [110] can also benefit from the experimental techniques employed in the proposed physical RC system. For example, one can use the experimental setup involving SL waves excited on the surface of a flowing liquid to create artistic music effects [111]. This intriguing application returns us to the discussion of the nonlinear effects associated with our perception of sound and music (see the Introduction), thereby demonstrating a fundamental link between nonlinear dynamics, natural intelligence, and AI.

6. Conclusions

We demonstrated an experimental physical RC system that employs solitary waves to implement a biologically inspired nonlinear transformation of input data instead of large matrices of the random neural connections that are central to the traditional RC algorithm. Post-processing raw experimental data using a technically simple and inexpensive Arduino microcontroller, we built a practicable neuromorphic computer that costs less than USD 100 and consumes very little electric power compared with both standard digital computers and many commercial and experimental neuromorphic systems that employ electron and photonic devices to mimic the neurons.

While feasible fluidic microprocessors have been demonstrated [112], thus paving the way for the further optimisation, miniaturisation, and eventual commercialisation of the physical RC system demonstrated in this paper, we foresee the application of the ideas proposed in this work in neuromorphic systems designed to closely resemble a biological neuron [113]. Indeed, since a living organism contains a significant amount of water and, therefore, can respond to physical stimuli in a nonlinear-dynamical manner [114], it is plausible that an SL wave-based RC system can be implemented as an organic bio-fluid-based artificial neuron that can communicate with biological neurons to complement and enhance their natural functionality.

Last but not least, the SL-wave-based neuromorphic computing platform is remarkably technically simple and, at the same time, rich in physical effects. Therefore, it can be both further explored by scientists and used by high-school and undergraduate students to understand the principles of neuromorphic computing [115].

Supplementary Materials: The following Supporting Information can be downloaded at: https://www.mdpi.com/article/10.3390/dynamics4010007/s1, Video S1: Solitary-like waves excited on the surface of a flowing liquid film.

Funding: The author did not receive any funding to support this project.

Institutional Review Board Statement: Not applicable.

Informed Consent Statement: Not applicable.

Data Availability Statement: All data generated in this work are presented in this article. A computational code that demonstrates how the Arduino board was used in the experimental setup can be found following this link: https://github.com/IvanMaksymov/Arduino-RC- (accessed on 5 February 2024).

Acknowledgments: The author acknowledges useful discussions with Abbas Hussein and Andrey Pototsky.

Conflicts of Interest: The author declares no conflict of interest.

Abbreviations

The following abbreviations are used in this manuscript:

AI	artificial intelligence
DC	direct current
ESN	Echo State Network
FLOPS	floating point operations per second
KdV	Korteweg–de Vries
LSM	Liquid State Machine
MGTS	Mackey–Glass time series
RC	reservoir computing
RAM	random access memory
SL	solitary-like
UV	ultraviolet
USD	United States Dollar

References

1. Babloyantz, A. Chaotic Dynamics in Brain Activity. In *Dynamics of Sensory and Cognitive Processing by the Brain*; Başar, E., Ed.; Springer: Berlin/Heidelberg, Germany, 1988; pp. 196–202.
2. McKenna, T.M.; McMullen, T.A.; Shlesinger, M.F. The brain as a dynamic physical system. *Neuroscience* **1994**, *60*, 587–605. [CrossRef] [PubMed]
3. Korn, H.; Faure, P. Is there chaos in the brain? II. Experimental evidence and related models. *C. R. Biol.* **2003**, *326*, 787–840. [CrossRef] [PubMed]
4. Muratov, C.B. A quantitative approximation scheme for the traveling wave solutions in the Hodgkin-Huxley model. *Biophys. J.* **2000**, *79*, 2893–2901. [CrossRef] [PubMed]
5. Heimburg, T.; Jackson, A.D. On soliton propagation in biomembranes and nerves. *Proc. Natl. Acad. Sci. USA* **2005**, *102*, 9790–9795. [CrossRef] [PubMed]
6. Gonzalez-Perez, A.; Budvytyte, R.; Mosgaard, L.D.; Nissen, S.; Heimburg, T. Penetration of action potentials during collision in the median and lateral giant axons of invertebrate. *Phys. Rev. X* **2014**, *4*, 031047. [CrossRef]
7. Larios, F.O.; Tretyakov, N.P.; Agüero, M.A. Catastrophe and hysteresis by the emerging of soliton-like solutions in a nerve model. *J. Nonlinear Dyn.* **2014**, *2014*, 710152. [CrossRef]

8. Hady, A.E.; Machta, B.B. Mechanical surface waves accompany action potential propagation. *Nat. Commun.* **2015**, *6*, 6697. [CrossRef]
9. Engelbrecht, J.; Peets, T.; Tamm, K. Electromechanical coupling of waves in nerve fibres. *Biomech. Model. Mechanobiol.* **2018**, *17*, 1771–1783. [CrossRef]
10. Yu, J.J.; Young, E.D. Linear and nonlinear pathways of spectral information transmission in the cochlear nucleus. *Proc. Natl. Acad. Sci. USA* **2000**, *97*, 11780–11786. [CrossRef]
11. Escabí, M.A.; Schreiner, C.E. Nonlinear spectrotemporal sound analysis by neurons in the auditory midbrain. *J. Neurosci.* **2002**, *22*, 4114–4131. [CrossRef]
12. Levitin, D.J. *This Is Your Brain on Music: The Science of Human Obsession*; Dutton: Boston, MA, USA, 2006.
13. Carney, L.H.; McDonough, J.M. Nonlinear auditory models yield new insights into representations of vowels. *Atten. Percept. Psychophys.* **2019**, *81*, 1034–1046. [CrossRef]
14. Keshishian, M.; Akbari, H.; Khalighinejad, B.; Herrero, J.L.; Mehta, A.D.; Mesgarani, N. Estimating and interpreting nonlinear receptive field of sensory neural responses with deep neural network models. *eLife* **2020**, *9*, e53445. [CrossRef]
15. Cariani, P.A.; Delgutte, B. Neural correlates of the pitch of complex tones. I. Pitch and pitch salience. *J. Neurophysiol.* **1996**, *76*, 1698–1716. [CrossRef]
16. Janata, P. Electrophysiological Studies of Auditory Contexts. Ph.D. Thesis, The University of Oregon, Eugene, OR, USA, 1996.
17. Chialvo, D.R. How we hear what is not there: A neural mechanism for the missing fundamental illusion. *Chaos* **2003**, *13*, 1226–1230. [CrossRef]
18. Maass, W.; Natschläger, T.; Markram, H. Real-time computing without stable states: A new framework for neural computation based on perturbations. *Neural Comput.* **2002**, *14*, 2531–2560. [CrossRef]
19. Adamatzky, A. *Advances in Unconventional Computing. Volume 2: Prototypes, Models and Algorithms*; Springer: Berlin/Heidelberg, Germany, 2017.
20. Zhou, J.; Qian, H.; Lu, X.; Duan, Z.; Huang, H.; Shao, Z. Polynomial activation neural networks: Modeling, stability analysis and coverage BP-training. *Neurocomputing* **2019**, *359*, 227–240. [CrossRef]
21. Marković, D.; Mizrahi, A.; Querlioz, D.; Grollier, J. Physics for neuromorphic computing. *Nat. Rev. Phys.* **2020**, *2*, 499–510. [CrossRef]
22. Zhang, W.; Gao, B.; Tang, J.; Yao, P.; Yu, S.; Chang, M.F.; Yoo, H.J.; Qian, H.; Wu, H. Neuro-inspired computing chips. *Nat. Electron.* **2020**, *3*, 371–382. [CrossRef]
23. Liao, X.; Song, W.; Zhang, X.; Yan, C.; Li, T.; Ren, H.; Liu, C.; Wang, Y.; Zheng, Y. A bioinspired analogous nerve towards artificial intelligence. *Nat. Commun.* **2020**, *11*, 268. [CrossRef]
24. Hasani, R.; Amini, M.L.A.; Rus, D.; Grosu, R. Liquid time-constant networks. In Proceedings of the 35th AAAI Conference on Artificial Intelligence (AAAI-21), Virtual, 2–9 February 2021; pp. 7657–7666.
25. He, F.; Yang, Y. Nonlinear system identification of neural systems from neurophysiological signals. *Neuroscience* **2021**, *458*, 213–228. [CrossRef]
26. Nakajima, M.; Inoue, K.; Tanaka, K.; Kuniyoshi, Y.; Hashimoto, T.; Nakajima, K. Physical deep learning with biologically inspired training method: Gradient-free approach for physical hardware. *Nat. Commun.* **2022**, *13*, 7847. [CrossRef] [PubMed]
27. Lee, O.; Wei, T.; Stenning, K.D.; Gartside, J.C.; Prestwood, D.; Seki, S.; Aqeel, A.; Karube, K.; Kanazawa, N.; Taguchi, Y.; et al. Task-adaptive physical reservoir computing. *Nat. Mater.* **2023**, 23, 79–87. [CrossRef] [PubMed]
28. López-Pastor, V.; Marquardt, F. Self-learning machines based on Hamiltonian echo backpropagation. *Phys. Rev. X* **2023**, *13*, 031020. [CrossRef]
29. Krauhausen, I.; Coen, C.T.; Spolaor, S.; Gkoupidenis, P.; van de Burgt, Y. Brain-inspired organic electronics: Merging neuromorphic computing and bioelectronics using conductive polymers. *Adv. Funct. Mater.* **2023**, 2307729. [CrossRef]
30. Lukoševičius, M.; Jaeger, H. Reservoir computing approaches to recurrent neural network training. *Comput. Sci. Rev.* **2009**, *3*, 127–149. [CrossRef]
31. Nakajima, K.; Fisher, I. *Reservoir Computing*; Springer: Berlin/Heidelberg, Germany, 2021.
32. Cucchi, M.; Abreu, S.; Ciccone, G.; Brunner, D.; Kleemann, H. Hands-on reservoir computing: A tutorial for practical implementation. *Neuromorph. Comput. Eng.* **2022**, *2*, 032002. [CrossRef]
33. Gauthier, D.J.; Bollt, E.; Griffith, A.; Barbosa, W.A.S. Next generation reservoir computing. *Nat. Commun.* **2021**, *12*, 5564. [CrossRef]
34. Jaeger, H. *Short Term Memory in Echo State Networks*; GMD Report 152; German National Research Center for Information Technology: Berlin, Germany, 2001.
35. Jaeger, H.; Haas, H. Harnessing nonlinearity: Predicting chaotic systems and saving energy in wireless communication. *Science* **2004**, *304*, 78–80. [CrossRef]
36. Kirby, K.G. Context dynamics in neural sequential learning. In Proceedings of the Florida AI Research Symposium (FLAIRS), Pensacola Beach, FL, USA, May 1991; pp. 66–70.
37. Jaeger, H. Echo state network. *Scholarpedia* **2007**, *2*, 2330. [CrossRef]
38. Maksymov, I.S. Analogue and physical reservoir computing using water waves: Applications in power engineering and beyond. *Energies* **2023**, *16*, 5366. [CrossRef]

39. Lukoševičius, M. A Practical Guide to Applying Echo State Networks. In *Neural Networks: Tricks of the Trade, Reloaded*; Montavon, G., Orr, G.B., Müller, K.R., Eds.; Springer: Berlin/Heidelberg, Germany, 2012; pp. 659–686.
40. Dudas, J.; Carles, B.; Plouet, E.; Mizrahi, F.A.; Grollier, J.; Marković, D. Quantum reservoir computing implementation on coherently coupled quantum oscillators. *NPJ Quantum Inf.* **2023**, *9*, 64. [CrossRef]
41. Maksymov, I.S.; Pototsky, A.; Suslov, S.A. Neural echo state network using oscillations of gas bubbles in water. *Phys. Rev. E* **2021**, *105*, 044206. [CrossRef]
42. Lukoševičius, M.; Uselis, A. Efficient implementations of Echo State Network cross-validation. *Cogn. Comput.* **2021**. [CrossRef]
43. Rafayelyan, M.; Dong, J.; Tan, Y.; Krzakala, F.; Gigan, S. Large-scale optical reservoir computing for spatiotemporal chaotic systems prediction. *Phys. Rev. X* **2020**, *10*, 041037. [CrossRef]
44. Maksymov, I.S.; Pototsky, A. Reservoir computing based on solitary-like waves dynamics of liquid film flows: A proof of concept. *Europhys. Lett.* **2023**, *142*, 43001. [CrossRef]
45. Kitayama, K.I. Guiding principle of reservoir computing based on "small-world" network. *Sci. Rep.* **2022**, *12*, 16697. [CrossRef]
46. Kawai, Y.; Park, J.; Asada, M. Reservoir computing using self-sustained oscillations in a locally connected neural network. *Sci. Rep.* **2023**, *13*, 15532. [CrossRef] [PubMed]
47. Ikeda, S.; Awano, H.; Sato, T. Modular DFR: Digital delayed feedback reservoir model for enhancing design flexibility. *ACM Trans. Embed. Comput. Syst.* **2023**, *22*, 1–20. [CrossRef]
48. Soriano, M.C.; Ortín, S.; Keuninckx, L.; Appeltant, L.; Danckaert, J.; Pesquera, L.; van der Sande, G. Delay-based reservoir computing: Noise effects in a combined analog and digital implementation. *IEEE Trans. Neural Netw. Learn. Syst.* **2015**, *26*, 388–393. [CrossRef] [PubMed]
49. Stelzer, F.; Röhm, A.; Vicente, R.; Fischer, I.; Yanchuk, S. Deep neural networks using a single neuron: Folded-in-time architecture using feedback-modulated delay loops. *Nat. Commun.* **2021**, *12*, 5164. [CrossRef] [PubMed]
50. Bollt, E. On explaining the surprising success of reservoir computing forecaster of chaos? The universal machine learning dynamical system with contrast to VAR and DMD. *Chaos* **2021**, *31*, 013108. [CrossRef]
51. Barbosa, W.A.S.; Gauthier, D.J. Learning spatiotemporal chaos using next-generation reservoir computing. *Chaos* **2022**, *32*, 093137. [CrossRef]
52. Kuan, R.; Wo-Yu, Z.; Fei, W.; Ze-Yu, G.; Da-Shan, S. Next-generation reservoir computing based on memristor array. *Acta Phys. Sin.* **2022**, *71*, 140701.
53. Liu, S.; Xiao, J.; Yan, Z.; Gao, J. Noise resistance of next-generation reservoir computing: A comparative study with high-order correlation computation. *Nonlinear Dyn.* **2023**, *111*, 14295–14308. [CrossRef]
54. Zhang, H.; Vargas, D.V. A survey on reservoir computing and its interdisciplinary applications beyond traditional machine learning. *IEEE Access* **2023**, *11*, 81033–81070. [CrossRef]
55. Ma, H.; Prosperino, D.; Räth, C. A novel approach to minimal reservoir computing. *Sci. Rep.* **2023**, *13*, 12970. [CrossRef] [PubMed]
56. Govia, L.C.G.; Ribeill, G.J.; Rowlands, G.E.; Ohki, T.A. Nonlinear input transformations are ubiquitous in quantum reservoir computing. *Neuromorph. Comput. Eng.* **2022**, *2*, 014008. [CrossRef]
57. Kosevich, Y.A. Nonlinear sinusoidal waves and their superposition in anharmonic lattices. *Phys. Rev. Lett.* **1993**, *71*, 2058–2061. [CrossRef] [PubMed]
58. Riou, M.; Torrejon, J.; Garitaine, B.; Araujo, F.A.; Bortolotti, P.; Cros, V.; Tsunegi, S.; Yakushiji, K.; Fukushima, A.; Kubota, H.; et al. Temporal pattern recognition with delayed-feedback spin-torque nano-oscillators. *Phys. Rep. Appl.* **2019**, *12*, 024049. [CrossRef] [PubMed]
59. Watt, S.; Kostylev, M. Reservoir computing using a spin-wave delay-line active-ring resonator based on yttrium-iron-garnet film. *Phys. Rev. Appl.* **2020**, *13*, 034057. [CrossRef]
60. Govia, L.C.G.; Ribeill, G.J.; Rowlands, G.E.; Krovi, H.K.; Ohki, T.A. Quantum reservoir computing with a single nonlinear oscillator. *Phys. Rev. Res.* **2021**, *3*, 013077. [CrossRef]
61. Götting, N.; Lohof, F.; Gies, C. Exploring quantumness in quantum reservoir computing. *Phys. Rev. A* **2023**, *108*, 052427. [CrossRef]
62. Cowan, G.E.R.; Melville, R.C.; Tsividis, Y.P. A VLSI analog computer/math co-processor for a digital computer. In Proceedings of the ISSCC. 2005 IEEE International Digest of Technical Papers. Solid-State Circuits Conference, San Francisco, CA, USA, 10 February 2005; Volume 1, pp. 82–586. [CrossRef]
63. Sorokina, M. Multidimensional fiber echo state network analogue. *J. Phys. Photonics* **2020**, *2*, 044006. [CrossRef]
64. Coulombe, J.C.; York, M.C.A.; Sylvestre, J. Computing with networks of nonlinear mechanical oscillators. *PLoS ONE* **2017**, *12*, e0178663. [CrossRef] [PubMed]
65. Fernando, C.; Sojakka, S. Pattern Recognition in a Bucket. In *Advances in Artificial Life, Proceedings of the 7th European Conference, ECAL 2003, Dortmund, Germany, 14–17 September 2003*; Banzhaf, W., Ziegler, J., Christaller, T., Dittrich, P., Kim, J.T., Eds.; Springer: Berlin/Heidelberg, Germany, 2003; pp. 588–597.
66. Gao, C.; Gaur, P.; Rubin, S.; Fainman, Y. Thin liquid film as an optical nonlinear-nonlocal medium and memory element in integrated optofluidic reservoir computer. *Adv. Photonics* **2022**, *4*, 046005. [CrossRef]
67. Marcucci, G.; Caramazza, P.; Shrivastava, S. A new paradigm of reservoir computing exploiting hydrodynamics. *Phys. Fluids* **2023**, *35*, 071703. [CrossRef]

68. Adamatzky, A. A brief history of liquid computers. *Philos. Trans. R. Soc. B* **2019**, *374*, 20180372. [CrossRef] [PubMed]
69. Sharma, S.; Marcucci, G. From Navier-Stokes millennium-prize problem to soft matter computing. *arXiv* **2022**, arXiv:2212.01492.
70. Sorokina, M.; Sergeev, S.; Turitsyn, S. Fiber echo state network analogue for high-bandwidth dual-quadrature signal processing. *Opt. Express* **2019**, *27*, 2387–2395. [CrossRef]
71. Jiang, J.; Lai, Y.C. Model-free prediction of spatiotemporal dynamical systems with recurrent neural networks: Role of network spectral radius. *Phys. Rev. Res.* **2019**, *1*, 033056. [CrossRef]
72. Zeng, Q.; Wu, Z.; Yue, D.; Tan, X.; Tao, J.; Xia, G. Performance optimization of a reservoir computing system based on a solitary semiconductor laser under electrical-message injection. *Appl. Opt.* **2020**, *59*, 6932–6938. [CrossRef]
73. Marcucci, G.; Pierangeli, D.; Conti, C. Theory of neuromorphic computing by waves: Machine learning by rogue waves, dispersive shocks, and solitons. *Phys. Rev. Lett.* **2020**, *125*, 093901. [CrossRef]
74. Silva, N.A.; Ferreira, T.D.; Guerreiro, A. Reservoir computing with solitons. *New J. Phys.* **2021**, *23*, 023013. [CrossRef]
75. Remoissenet, M. *Waves Called Solitons: Concepts and Experiments*; Springer: Berlin/Heidelberg, Germany, 1994.
76. Maksymov, I.S.; Pototsky, A. Solitary-like wave dynamics in thin liquid films over a vibrated inclined plane. *Appl. Sci.* **2022**, *13*, 1888. [CrossRef]
77. Pototsky, A.; Maksymov, I.S. Nonlinear periodic and solitary rolling waves in falling two-layer viscous liquid films. *Phys. Rev. Fluids* **2023**, *8*, 064801. [CrossRef]
78. Liu, J.; Gollub, J.P. Solitary wave dynamics of film flows. *Phys. Fluids* **1994**, *6*, 1702–1712. [CrossRef]
79. Korteweg, D.J.; De Vries, G. On the change of form of long waves advancing in a rectangular canal, and on a new type of long stationary waves. *Philos. Mag.* **1895**, *39*, 422–443. [CrossRef]
80. Trouvain, N.; Pedrelli, L.; Dinh, T.T.; Hinaut, X. ReservoirPy: An Efficient and User-Friendly Library to Design Echo State Networks. In Proceedings of the ICANN 2020-29th International Conference on Artificial Neural Networks, Bratislava, Slovakia, 15–18 September 2020.
81. Balmforth, N.J.; Mandre, S. Dynamics of roll waves. *J. Fluid Mech.* **2004**, *514*, 1–33. [CrossRef]
82. Maksymov, I.S.; Greentree, A.D. Coupling light and sound: Giant nonlinearities from oscillating bubbles and droplets. *Nanophotonics* **2019**, *8*, 367–390. [CrossRef]
83. Kurkina, O.; Pelinovsky, E. Nonlinear transformation of sine wave within the framework of symmetric (2+4) KdV equation. *Symmetry* **2022**, *14*, 668. [CrossRef]
84. Jenkins, A. Self-oscillation. *Phys. Rep.* **2013**, *525*, 167–222. [CrossRef]
85. Shougat, M.R.E.U.; Perkins, E. The van der Pol physical reservoir computer. *Neuromorph. Comput. Eng.* **2023**, *3*, 024004. [CrossRef]
86. Rodan, A.; Tino, P. Minimum complexity Echo State Network. *IEEE Trans. Neural Netw.* **2011**, *22*, 131–144. [CrossRef] [PubMed]
87. Morales, G.B.; Mirasso, C.R.; Soriano, M.C. Unveiling the role of plasticity rules in reservoir computing. *Neurocomputing* **2021**, *461*, 705–715. [CrossRef]
88. Lorenz, E.N. Deterministic nonperiodic flow. *J. Atmos. Sci.* **1963**, *20*, 130–141. [CrossRef]
89. Rössler, O.E. An equation for continuous chaos. *Phys. Lett.* **1976**, *57A*, 397–398. [CrossRef]
90. Hénon, M. A two-dimensional mapping with a strange attractor. *Commun. Math. Phys.* **1976**, *50*, 69–77. [CrossRef]
91. Ikeda, K. Multiple-valued stationary state and its instability of the transmitted light by a ring cavity system. *Opt. Commun.* **1979**, *30*, 257–261. [CrossRef]
92. Mackey, M.C.; Glass, L. Oscillation and chaos in physiological control systems. *Science* **1977**, *197*, 287–289. [CrossRef]
93. Kan, S.; Nakajima, K.; Asai, T.; Akai-Kasaya, M. Physical implementation of reservoir computing through electrochemical reaction. *Adv. Sci.* **2022**, *9*, 2104076. [CrossRef]
94. van der Made, P. Learning How to Learn: Neuromorphic AI Inference at the Edge. BrainChip White Paper. 2022, p. 12. Available online: https://brainchip.com/wp-content/uploads/2022/08/BrainChip-Learning-how-to-Learn.pdf (accessed on 1 January 2023).
95. Mehonic, A.; Kenyon, A.J. Brain-inspired computing needs a master plan. *Nature* **2022**, *604*, 255–260. [CrossRef]
96. Kheirabadi, N.R.; Chiolerio, A.; Szaciłowski, K.; Adamatzky, A. Neuromorphic liquids, colloids, and gels: A review. *ChemPhysChem* **2023**, *24*, e202200390. [CrossRef] [PubMed]
97. Karimov, A.; Kopets, E.; Karimov, T.; Almjasheva, O.; Arlyapov, V.; Butusov, D. Empirically developed model of the stirring-controlled Belousov–Zhabotinsky reaction. *Chaos Solitons Fractals* **2023**, *176*, 114149. [CrossRef]
98. Shastri, B.J.; Tait, A.N.; de Lima, T.F.; Pernice, W.H.P.; Bhaskaran, H.; Wright, C.D.; Prucnal, P.R. Photonics for artificial intelligence and neuromorphic computing. *Nat. Photonics* **2020**, *15*, 102–114. [CrossRef]
99. Lin, X.; Yang, Z.; Song, Y. Short-term stock price prediction based on echo state networks. *Expert Syst. Appl.* **2009**, *36*, 7313–7317. [CrossRef]
100. Sun, G.; Lin, J.; Yang, C.; Yin, X.; Li, Z.; Sun, P.G.J.; Fan, X.; Pan, B. Stock price forecasting: An Echo State Network approach. *Comput. Syst. Sci. Eng.* **2021**, *36*, 509–520. [CrossRef]
101. Lillo, F.; Mantegna, R.N. Variety and volatility in financial markets. *Phys. Rev. E* **2000**, *62*, 6126–6134. [CrossRef] [PubMed]
102. Kawai, Y.; Park, J.; Asada, M. A small-world topology enhances the echo state property and signal propagation in reservoir computing. *Neural Netw.* **2019**, *112*, 15–23. [CrossRef] [PubMed]
103. Suárez, L.E.; Richards, B.A.; Lajoie, G.; Misic, B. Learning function from structure in neuromorphic networks. *Nat. Mach. Intell.* **2021**, *3*, 771–786. [CrossRef]

104. Damicelli, F.; Hilgetag, C.C.; Goulas, A. Brain connectivity meets reservoir computing. *PLoS Comput. Biol.* **2022**, *18*, e1010639. [CrossRef]
105. Rao, A.; Plank, P.; Wild, A.; Maass, W. A long short-term memory for AI applications in spike-based neuromorphic hardware. *Nat. Mach. Intell.* **2022**, *4*, 467–479. [CrossRef]
106. Sporns, O. The non-random brain: Efficiency, economy, and complex dynamics. *Front. Comput. Neurosci.* **2011**, *5*, 5. [CrossRef]
107. Saha, S.; Mamun, K.A.; Ahmed, K.; Mostafa, R.; Naik, G.R.; Darvishi, S.; Khandoker, A.H.; Baumert, M. Progress in brain computer interface: Challenges and opportunities. *Front. Syst. Neurosci.* **2021**, *15*, 578875. [CrossRef]
108. Papp, A.; Porod, W.; Csaba, G. Nanoscale neural network using non-linear spin-wave interference. *Nat. Commun.* **2021**, *12*, 6422. [CrossRef] [PubMed]
109. Nakane, R.; Hirose, A.; Tanaka, G. Performance enhancement of a spin-wave-based reservoir computing system utilizing different physical conditions. *Phys. Rev. Appl.* **2023**, *19*, 034047. [CrossRef]
110. Maksymov, I.S. Artificial musical creativity enabled by nonlinear oscillations of a bubble acting as a physical reservoir computing system. *Int. J. Unconv. Comput.* **2023**, *18*, 269–289.
111. Lauterwasser, A. *Water Sound Images: The Creative Music of the Universe*; MACROmedia: San Francisco, CA, USA, 2007.
112. Lee, W.; Yu, M.; Lim, D.; Kang, T.; Song, Y. Programmable DNA-based Boolean logic microfluidic processing unit. *ACS Nano* **2021**, *15*, 11644–11654. [CrossRef] [PubMed]
113. Sarkar, T.; Lieberth, K.; Pavlou, A.; Frank, T.; Mailaender, V.; McCulloch, I.; Blom, P.W.M.; Torricelli, F.; Gkoupidenis, P. An organic artificial spiking neuron for in situ neuromorphic sensing and biointerfacing. *Nat. Electron.* **2022**, *5*, 774–783. [CrossRef]
114. Maksymov, I.; Pototsky, A. Excitation of Faraday-like body waves in vibrated living earthworms. *Sci. Rep.* **2020**, *10*, 8564. [CrossRef] [PubMed]
115. Roumen, G.J.; Fernaeus, Y. Envisioning Arduino action: A collaborative tool for physical computing in educational settings. *Int. J. Child Comput. Interact.* **2021**, *29*, 100277. [CrossRef]

Disclaimer/Publisher's Note: The statements, opinions and data contained in all publications are solely those of the individual author(s) and contributor(s) and not of MDPI and/or the editor(s). MDPI and/or the editor(s) disclaim responsibility for any injury to people or property resulting from any ideas, methods, instructions or products referred to in the content.